

Secuer: ultrafast, scalable and accurate clustering of single-cell RNA-seq data

Nana Wei¹, Yating Nie¹, Lin Liu², Xiaoqi Zheng^{3,*}, Hua-Jun Wu^{4,*}

¹Department of Mathematics, Shanghai Normal University, Shanghai, China. ²Institute of Natural Sciences, MOE-LSC, School of Mathematical Sciences, CMA-Shanghai, SJTU-Yale Joint Center for Biostatistics and Data Science, Shanghai Jiao Tong University, Shanghai, China. ³Center for Single-Cell Omics, School of Public Health, Shanghai Jiao Tong University School of Medicine, Shanghai, China. ⁴Center for Precision Medicine Multi-Omics Research, School of Basic Medical Sciences, Peking University Health Science Center and Peking University Cancer Hospital and Institute, Beijing, China.

* **Correspondence:** hjwu@pku.edu.cn; xqzheng@shnu.edu.cn

ABSTRACT

Identifying cell clusters is a critical step for single-cell transcriptomics study. Despite the numerous clustering tools developed recently, the rapid growth of scRNA-seq volumes prompts for a more (computationally) efficient clustering method. Here, we introduce Secuer, a Scalable and Efficient speCtral cUstERing algorithm for scRNA-seq data. By employing an anchor-based bipartite graph representation algorithm, Secuer enjoys reduced runtime and memory usage by orders of magnitude, especially for ultra-large datasets profiling over 1 or even 10 million cells. Meanwhile, Secuer also achieves better or comparable accuracy than competing methods in small and moderate benchmark datasets. Furthermore, we showcase that Secuer can also serve as a building block for a new consensus clustering method, Secuer-consensus, which again greatly improves the runtime and scalability of state-of-the-art consensus clustering methods while also maintaining the accuracy. Overall, Secuer is a versatile, accurate, and scalable clustering framework suitable for small to ultra-large single-cell clustering tasks.

In the past decade, single-cell RNA sequencing (scRNA-seq) has transformed our understanding of development and disease through profiling the whole transcriptome at the cellular level^{1,2}. It has been widely used to unravel cell-to-cell heterogeneity and gain new biological insights, owing to its ability to identify and characterize cell types in complex tissues³. Unsupervised clustering approaches have played a central role in determining cell types. However, the scale of scRNA-seq experiments has been rapidly climbing in recent years, amounting to several datasets profiling over 1 million cells^{4,5}. The increasing sample size renders many of the existing scRNA-seq clustering

algorithms obsolete and prompts for developing a new generation of clustering algorithms that are efficient and scalable to large (500,000 ~ 5 million) or even ultra-large (> 5 million) scRNA-seq datasets.

Currently, two clustering algorithms, Louvain and Leiden, prevail in scRNA-seq analysis and have recently been implemented in numerous tools such as Seurat and Scanpy^{6, 7}. Both algorithms aim to partition a graph into connected subgraphs by iteratively aggregating nodes: Louvain infers clusters by maximizing modularity⁸, and Leiden is a variant of Louvain by using a local node-moving technique⁹. However, both algorithms are not well scaled to ultra-large datasets. For instance, for a dataset consisting of 10 million cells, Louvain and Leiden usually take 45 minutes and more than 1 hour for clustering, and both unreliably and unreasonably overestimate the number of clusters (as many as 1 million, see details in the Result section).

To address this gap, we present Secuer, a superfast and scalable clustering algorithm for (ultra-)large scRNA-seq data analysis based on spectral clustering. Spectral clustering has been one of the most popular clustering techniques due to its ease of use and flexibility of handling data with complicated shape or distribution¹⁰, but with the caveat of high computational cost. We tailor the conventional spectral clustering to large scRNA-seq data by leveraging the following three key elements in Secuer: First, we pivot p anchors from all N cells ($p \ll N$) and construct a weighted bipartite graph between cells and anchors by a modified approximate k -nearest neighbor (MAKNN) algorithm, which greatly accelerates the runtime of our method. Second, we determine the weights of the bipartite graph by a locally-scaled Gaussian kernel function to capture the local geometry of the cell-to-anchor similarity network, which improves the accuracy of our method. Third, we design two optional approaches to automatically infer the number of clusters -- K , which avoids manually choosing some K by users.

We evaluate Secuer against three extensively used methods for scRNA-seq clustering including Louvain, Leiden, and k-means, using 31 simulated datasets with the number of cells ranging from 10,000 to 40 million. Secuer utilizes much shorter runtime than existing methods without deteriorating the clustering accuracy. In particular, Secuer is 5 times faster than k-means and 12 times faster than Louvain/Leiden for ultra-large datasets. Moreover, Secuer infers the number of clusters in the anchor space. The cluster number estimates by Secuer are still accurate when the sample size is larger than 5 million, in which case both Louvain and Leiden fail to produce any reasonable estimates. We then evaluate all the aforementioned methods in 15 real datasets with the number of cells ranging from 49 to 1.46 million (**Supplementary Table 1**), and find that Secuer yields more or comparably accurate clustering results than the other methods, and saves 90% of runtime in general.

With Secuer as a subroutine, we also develop a consensus clustering method, Secuer-consensus, by aggregating multiple clustering results obtained by Secuer to further boost clustering accuracy and stability. Compared to the popular consensus clustering algorithm SC3⁷, Secuer-consensus attains better clustering accuracy on twelve gold/silver standard datasets, is in general 100 times faster, and can work on large datasets in which SC3 even fails to produce any useful output. In summary, Secuer

and Secuer-consensus are accurate and scalable algorithms that provide a general framework for efficient (consensus) clustering of small to ultra-large scRNA-seq datasets that are being produced by a growing array of single cell transcriptomic projects.

Results

Overview of Secuer. The workflow of Secuer is illustrated in Fig. 1. To improve computational efficiency, Secuer starts by randomly sampling a subset of p' (10,000 by default) cells from all N cells (**Fig. 1a, b**). p anchors are then obtained, which are the centroids of the identified clusters by applying k-means to the above random subsample (**Fig. 1b**). Next the k -nearest anchors of all cells are determined by the MAKNN algorithm (**Fig. 1c**; see Methods). Then, a weighted bipartite graph between anchors and cells is constructed, with similarities between anchors and cells quantified by a locally-scaled Gaussian kernel (see Methods) to better capture the local geometry of the gene expression landscape (**Fig 1d**). Finally, we compute the first K eigenvectors of the graph Laplacian by transfer cuts (T-cut) algorithm and obtain the final clustering results by off-the-shelf clustering algorithms such as k-means (by default) (**Fig. 1e**). Secuer also automatically infers the number of clusters by either applying a community detection-based technique on the graph of the anchors (**Fig. 1f**), or using the number of near-zero eigenvalues of the graph Laplacian (see Methods).

We observed that the locally-scaled Gaussian kernel is better suited to scRNA-seq data than the traditional Gaussian kernel on certain datasets (**Supplementary Fig. 1**). In addition, we studied how two important tuning parameters – p (the number of anchors) and k (the number of nearest neighbors in MAKNN) – affected the clustering results in Secuer, and found that $p = 1000$ and $k = 7$ produced superior results (**Supplementary Fig. 4**), which are therefore recommended as the default values when implementing Secuer.

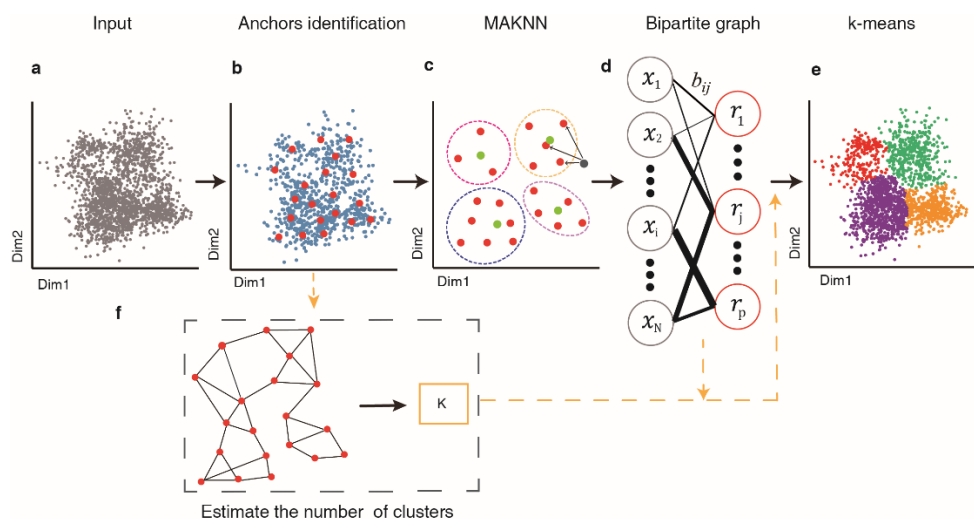


Fig. 1 Overview of the Secuer algorithm. **a**, Secuer takes the matrix in which rows are cells and columns are features as input. **b**, Secuer obtains p anchors (red points) by using k-means on a random subset of p' cells from all N cells (blue points). **c**, The MAKNN algorithm step aims to

find the k nearest anchors for each cell (green points). **d**, A weighted bipartite graph is constructed, with nodes representing cells (denoted as x) and anchors (denoted as r) and weights computed by a locally-scaled Gaussian kernel distance. **e**, Secuer applies k-means to the eigenvectors of the graph Laplacian of the weighted bipartite graph to obtain the final clustering results. **f**, Secuer estimates the number of clusters based on the graph of the anchors or based on the eigenvalues of the graph Laplacian of the weighted bipartite graph of cells and anchors.

Secuer performance on simulated datasets. Clustering ultra-large scRNA-seq datasets is computationally intensive in terms of both runtime and memory usage. We generated a series of scRNA-seq datasets with an increasing number of cells ranging from 10,000 to 40 million (see Methods) to test the performance of Secuer and three widely used clustering methods: k-means, Louvain and Leiden. The number of clusters is determined by the default parameters except for k-means. For the ease of comparison, the reference/ground-truth (see Methods) number of clusters are given to k-means as input. The clustering accuracy is measured by the Adjusted Rand Index (ARI)¹¹ and the Normalized Mutual Information (NMI)¹².

First, we compared the runtimes of different methods. Secuer is the fastest on large and ultra-large datasets, in particular for ultra-large datasets, where Secuer is 5 times faster than k-means, and 12 times faster than Louvain/Leiden. Though k-means is faster for small datasets, the runtime only differs slightly from Secuer (below 10 seconds) (**Fig. 2a**). In contrast, Louvain and Leiden are much slower than Secuer and k-means when applied to datasets over all scales, and fail to process the datasets of more than 10 million cells (**Fig. 2a**). Note the runtime of Louvain and Leiden does not monotonically increase with the sample size, possibly due to the much higher number of estimated clusters for larger datasets (**Fig. 2c**). We then investigated the memory usage of different methods. It appears that Secuer and k-means consume the least amount of memory in all datasets. In comparison to Louvain and Leiden, Secuer only requires one-tenth of their memory usage when the sample size is over 1 million (**Fig. 2b**). We also evaluated the clustering accuracy of all the methods and found that they all performed similarly when the sample sizes are less than 5 million. However, Louvain and Leiden performed poorly when there are more than 5 million cells, suggesting that they should not be applied directly to ultra-large datasets, even without concerning the computational cost (**Supplementary Fig. 2a**).

Next, we investigated the accuracy of Secuer in inferring the number of clusters (K). We set the true $K = 19$ across all simulated datasets over different sample sizes (see Methods). Fig. 2c displays the number of clusters identified by Secuer, Louvain and Leiden, with sample sizes varying from 10,000 to 40 million. The numbers of clusters estimated by Secuer only fluctuate mildly around 18 across different simulations. However, neither Louvain nor Leiden can infer K correctly in large datasets when the number of cells is over 5 million (**Fig. 2c**). Notably, the estimated numbers of clusters by Louvain and Leiden are enormously upwardly biased, and such a bias cannot be easily fixed by simply lowering the resolution parameter to 0.0001 (**Supplementary Fig. 2b**). This further suggests that Secuer should be favored over Louvain and Leiden when analyzing large to ultra-large datasets.

Finally, we compared Secuer with the vanilla spectral clustering algorithms (VSC), especially in runtime. To this end, we divided the clustering procedure into three steps: constructing weighted bipartite graph, solving the eigen-problem, and the final clustering. We investigated the runtime of each step between Secuer and VSC. Secuer has significantly reduced runtime on the graph construction step in larger datasets and the eigen-solving step in datasets over all scales, due to the use of the T-cut algorithm on the anchor-based bipartite graph (**Supplementary Fig. 2c, d**, see Methods).

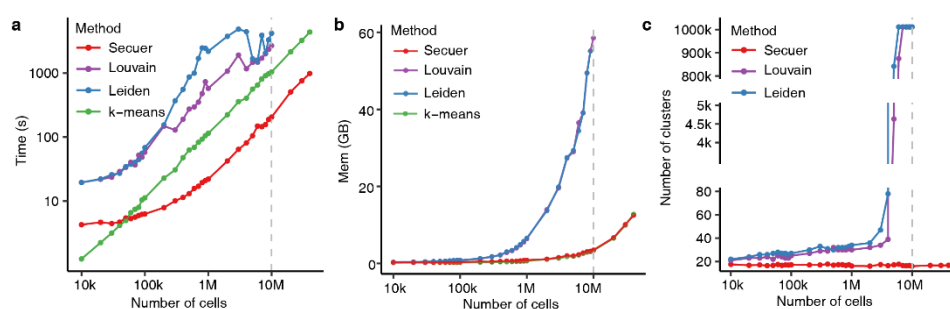


Fig. 2 The performance of runtime and estimated number of clusters in the simulated datasets. **a**, The clustering runtime vs. the number of cells in the simulated datasets for all four methods. **b**, The memory usage vs. the number of cells in the simulated datasets for all four methods. **c**, The estimated number of clusters vs. the number of cells in the simulated datasets for three out of four methods: Secuer, Louvain and Leiden. k: thousand, M: million.

Secuer performance on large real datasets. To evaluate the performance of our method on large real datasets, we collected three scRNA-seq datasets recently reported: COVID-19 dataset profiling 1.46 million immune cells isolated from 196 patients; MCA dataset containing 325,486 cells from multiple major mouse organs; and Mouse Brain dataset consisting of over 1 million cells from two E18 mice. For each dataset, we performed all clustering methods 10 times and reported the average runtimes and clustering accuracy.

Secuer has the shortest runtime on all datasets (**Fig. 3a**). In particular, for the COVID-19 dataset with more than 1 million cells, the runtime of Secuer is < 1 minute on average, which is 3 times faster than k-means, and 24 times faster than Louvain and Leiden. In the meanwhile, Secuer achieves competitive accuracy in general compared to other methods measured by both ARI (**Fig. 3b**) and NMI (**Supplementary Fig. 3c**). An example of the clustering results by all methods are displayed in Uniform Manifold Approximation and Projection (UMAP)¹³ visualization (**Fig. 3c-i**), in which the cell type labels are obtained from Xie et al.¹⁴. Under default parameters, Secuer exhibits more apparent cell type separations than Louvain and Leiden, both of which obtain 1.5 times more clusters showing ambiguous patterns, especially on the right region of the plot with a lot of small clusters overlaying with each other (**Fig. 3d-f**). The performance of Louvain and Leiden is improved when the number of clusters is tuned to be the same as that of Secuer. However, by doing this they fail to distinguish the Interneurons (cluster 1 in Secuer) and Neural stem/precursor cells (cluster 6 in Secuer) in the lower left corner of the plot (**Fig. 3g, h**). Likewise, k-means also fail to distinguish the two

clusters even though the original number of cell type labels is given (**Fig. 3i**). Taken together, these findings demonstrate that Secuer is an efficient and accurate algorithm for clustering large scRNA-seq datasets.

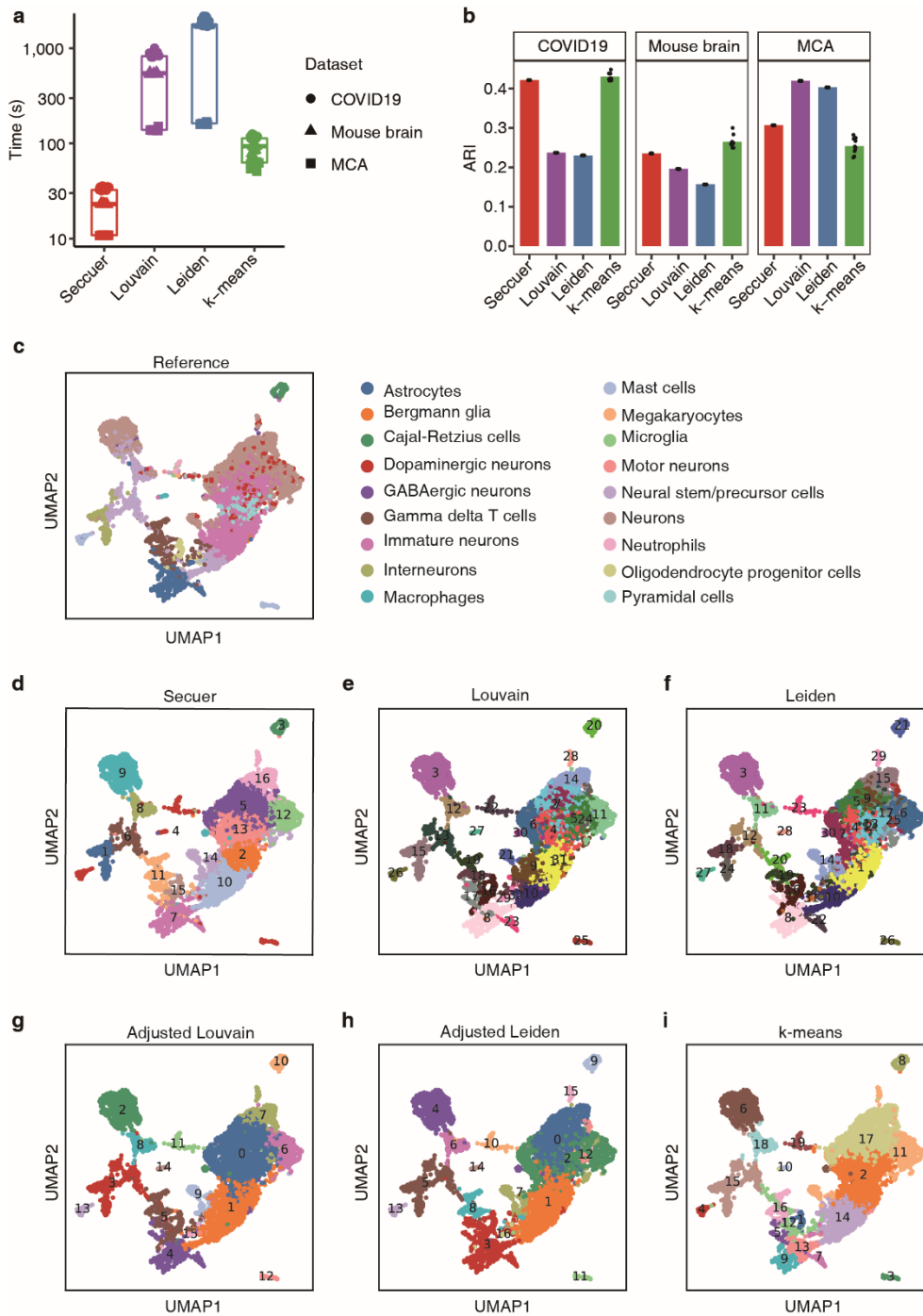


Fig. 3 The performance of different methods on large real datasets. **a**, The clustering time of different methods. **b**, The ARI of different methods on three large datasets. **c-i**, UMAP visualization of the Mouse brain dataset for the different methods. Reference (**c**) illustrates the ground-truth cell type labels obtained from the original study. Secuer (**d**), Louvain (**e**), and Leiden (**f**) display clustering results by using their default parameters. Adjusted Louvain (**g**) and adjusted Leiden (**h**)

refer to the clustering results by setting the resolution parameter to 0.3. k-means (i) represents the clustering results given the ground-truth number of clusters in (c).

Secuer performance on well-annotated benchmark datasets. To further investigate the performance of our method in large scale benchmark datasets, we applied the same analyses as above on six gold standard and six silver standard scRNA-seq datasets introduced by SC3⁷, scDCC¹⁵, and MARS⁴. These datasets, with numbers of cells varying from 49 to 110,832, are widely used to benchmark the performance of new clustering methods because the cell type labels with high confidence are available.

As expected, Secuer and k-means remain to have the shortest runtimes, which are at least 10 times faster than Louvain and Leiden across all 12 datasets (**Fig. 4a**). In terms of accuracy, Secuer outperforms Louvain and Leiden on 7 out of 12 datasets (mean ARI difference > 0.05), and is substantially better on 4 out of 12 (Goolam, Biase, Human kidney and Mouse retina, mean ARI difference > 0.2) (**Fig. 4b, c**). The distribution of ARI across all datasets demonstrates that Secuer is highly competitive even only in terms of clustering accuracy (**Fig. 4d**). Likewise, similar trends are observed when measuring accuracy using NMI (**Supplementary Fig. 3**). k-means sometimes achieves better accuracy than the other methods, but the clustering results are exceedingly inconsistent across different initializations. For instance, the range of ARI in different runs is 0.5 in the Biase dataset (**Fig. 4b**). Furthermore, we found that k-means is sensitive to changes in the data preprocessing pipelines. In most cases, the mean NMIs of k-means with and without preprocessing step differ by a large margin, especially for Goolam and CITE PBMC datasets (mean NMI difference > 0.5 , **Supplementary Fig. 6**). Using the Mouse retina dataset as an example, The UMAP visualization suggests that the clusters inferred by Secuer are more aligned with the given reference cell-type annotations (**Fig. 4e-i**), regarded as the ground truth. Notably, cluster 1 identified by Secuer is perfectly matched with the reference cluster 5, but none of the other approaches are capable of recovering this reference cluster. Finally, we examined the accuracy of the estimated number of clusters by different methods on all 12 datasets and discovered that Secuer outperformed Louvain and Leiden (**Supplementary Fig. 5**). These results demonstrate that Secuer is also competitive in terms of clustering accuracy for small and moderate scRNA-seq datasets.

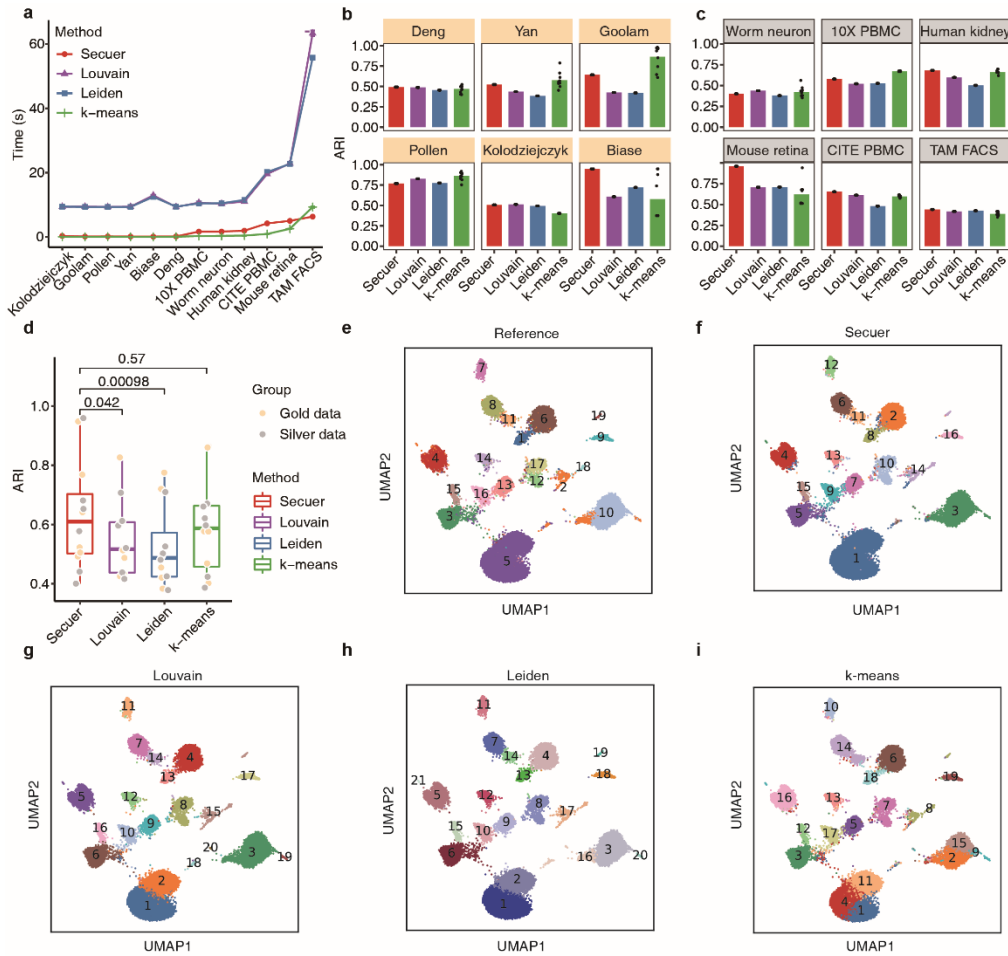


Fig. 4 Performance of Secuer in twelve gold and silver standard datasets. a, The clustering runtime of each method on all twelve datasets. **b-c**, Accuracy of different methods, including k-means, Louvain, Leiden, and Secuer, on gold (**b**) and silver (**c**) standard datasets. **d**, A boxplot showing the distribution of ARI of different methods on all datasets. **e-i**, UMAP visualization of the ground-true cell type labels obtained from the original study, termed as reference (**e**) and clustering results from four different methods (**f-i**) on Mouse retina dataset.

Secuer-consensus performance on well-annotated benchmark datasets. Most of the unsupervised clustering algorithms may yield inconsistent results due to random initialization and different parameter settings. To resolve this common problem, consensus clustering aggregates multiple outputs generated by different clustering algorithms or by the same algorithm but with varied parameter settings, to produce consensus clusters that are expected to be more stable and accurate⁷. Just as in the case of usual clustering, consensus clustering method applicable to large-scale scRNA-seq data is also lacking. To bridge this gap, with Secuer as a subroutine, we developed Secuer-consensus, a highly efficient consensus clustering algorithm that ensembles multiple outputs of Secuer by fully taking advantage of its computational efficiency. The implementation of Secuer-consensus constitutes three steps (**Fig. 5a**): First, Secuer is run for M times with different distance metrics, including Euclidean and cosine distances, and different numbers of clusters estimated by different parameter settings to

generate multiple clustering outputs. Second, an unweighted bipartite graph is constructed from the multiple outputs. Third, k-means clustering is performed on the unweighted bipartite graph.

We evaluated the performance of Secuer-consensus on twelve gold/silver standard datasets by comparing it to the original Secuer and SC3, a widely used consensus clustering method. We studied how many clustering outputs of Secuer (M) should be fed into Secuer-consensus and found that setting M between 5 and 10 has generally better performance (**Supplementary Fig. 7**). Hence, we set $M = 5$ for all datasets hereafter. It can be found that Secuer-consensus is over 100 times faster than SC3 in all datasets (**Fig. 5b**). Notably, Secuer-consensus completes clustering within 1 second on average on the gold standard datasets, while SC3 takes more than 100 seconds. On the larger silver standard datasets, SC3 sometimes takes over 2 hours for processing the data, while Secuer-consensus only takes about 40 seconds. More importantly, Secuer-consensus succeeds in processing larger datasets with 27,499 and 110,832 single cells in 50 seconds, while SC3 fails. Regarding accuracy, Secuer-consensus is similar or superior to Secuer and SC3, depending on the datasets. Specifically, Secuer-consensus surpasses SC3 on 9 out of 10 datasets (mean ARI difference > 0.05), and substantially outperforms SC3 on four datasets (Biase, Goolam, Human kidney and CITE PBMC, mean ARI difference > 0.2) (**Fig. 5c**). These findings indicate that Secuer-consensus is an appealing option for consensus clustering small and moderate scRNA-seq datasets.

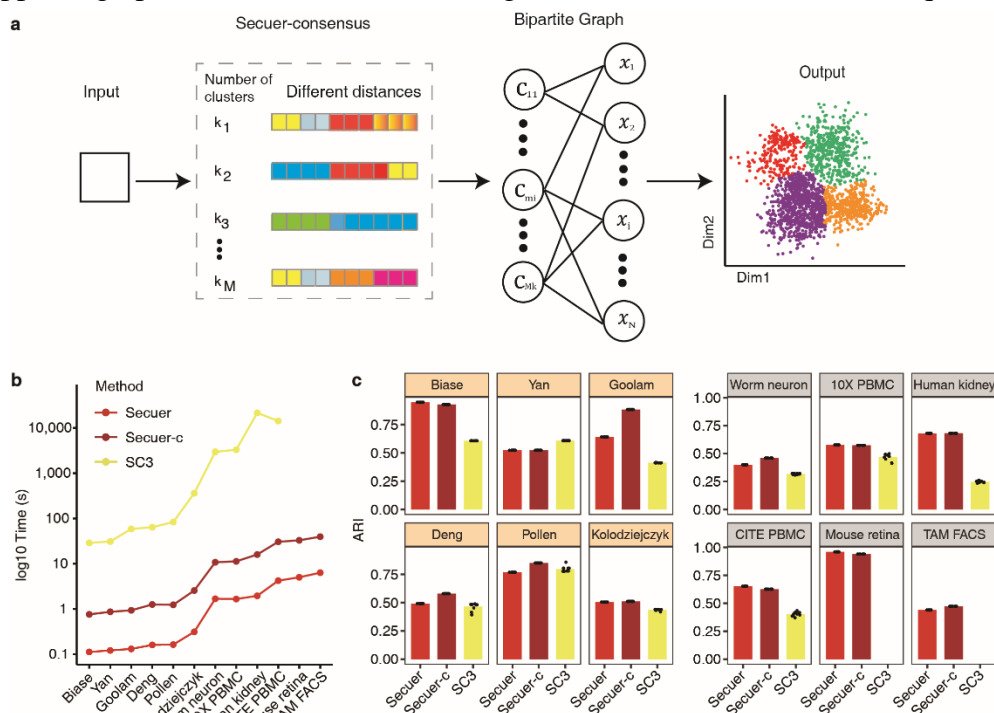


Fig. 5 Overview of the Secuer-consensus algorithm and the performance in twelve gold and silver standard scRNA-seq datasets. **a**, Secuer-consensus takes a matrix as input, with genes as the columns and cells as the rows, executes Secuer M times to acquire multiple clustering outputs, and constructs an unweighted bipartite graph, with two disjoint sets of nodes respectively representing the clusters (denoted as C) and cells (denoted as x). Finally, k-means clustering is used to obtain a consensus grouping. **b**, The clustering runtime for different methods. Secuer-c:

short for Secuer-consensus. **c**, The ARI for three methods on twelve gold/silver standard datasets.

Summary

Identifying cell clusters is a critical step for scRNA-seq data analysis. Computationally efficient and scalable methods are urgently needed due to the rapidly expanding volume of scRNA-seq data. In this work, we presented Secuer, a computationally efficient, ultra-scalable and accurate method for unsupervised clustering of scRNA-seq data. Secuer is on average 10 times faster than Louvain and Leiden while exhibiting similar accuracy in 15 benchmark datasets, covering different sequencing technologies, with the number of cells ranging from 49 to 1.4 million. Secuer can efficiently scale to ultra-large scRNA-seq datasets of more than 10 million cells, when neither Louvain nor Leiden is even able to process the data. For instance, Secuer can cluster a scRNA-seq dataset of 10 million cells within 2 minutes, which is 6 times faster than k-means, one of the most efficient off-the-shelf clustering algorithms. In addition, Secuer can reliably estimate the number of clusters regardless of the number of cells in the data, whereas both Louvain and Leiden usually erroneously identify > 0.9 million clusters for datasets with over 5 million cells.

With Secuer as a subroutine, we also proposed a consensus clustering method, Secuer-consensus, by aggregating multiple Secuer runs with an array of different parameter settings. Secuer-consensus surpasses or approaches Secuer and SC3 in all 12 benchmark datasets. Notably, Secuer-consensus only takes less than 1% the runtime of SC3. This allows Secuer-consensus to cluster cell types with improved stability and accuracy compared to the non-consensus-based methods, while being substantially more efficient than competitive consensus clustering methods, such as SC3.

Overall, our new clustering framework strikes a good balance between accuracy, computational cost and scalability. It is an appealing choice for clustering large-scale scRNA-seq atlas, and can also be easily incorporated into any online scRNA-seq computational platforms for real-time analysis. The computational efficiency of Secuer also makes it a building block for scalable consensus clustering, demonstrated by the superior performance of Secuer-consensus than other competing methods. Secuer is also flexible enough to be adapted to a wide range of clustering algorithms beyond spectral clustering, such as Louvain or upcoming new approaches, to enhance their efficiency and scalability. As the rapid development of droplet-based single cell technologies, we expect our framework can eventually be applied to identify cell clusters in large-scale omics data other than scRNA-seq, such as scATAC-seq, CyTOF and image-based spatial data.

Methods

Benchmark datasets. Fifteen publicly available scRNA-seq datasets, including six gold-standard datasets, six silver-standard datasets and three ultra-large datasets, are used to evaluate the clustering accuracy of our method (see Supplementary Table 1 for details)^{1, 5, 16-28}. In six gold-standard datasets, cells are highly confident to be labeled as a specific cell type/stage according to their surface markers. In six silver standard datasets, the label of each cell is assigned by computational tools and manual annotation

using prior knowledge by previous studies^{22-26, 28}. Although widely used to benchmark a newly proposed clustering method^{4, 7, 29}, these datasets are relatively small in size (containing from 49 to 110,832 cells per dataset), and thus insufficient to evaluate a method designed for much higher throughput considered in this paper. Thus, we also assessed our method using three large datasets^{5, 30}, which consist of 1 million cells on average. The cell type labels in these datasets are collected from the original studies. In all the 15 datasets, the cell type labels are considered as ground-truth, also termed as “reference”, throughout this study.

Data preprocessing. The preprocessing involves four steps: i) gene/cell filtering; ii) normalization; iii) selection of highly variable genes; iv) dimension reduction by PCA. The parameters of the preprocessing pipeline are the same for all datasets except for the first step, which instead follows the criteria in the original studies. For six small gold standard datasets, we adopted a preprocessing strategy of gene filtering similar to that for SC3⁷: genes are removed by the ‘gene filter’ function in the Scanpy package³¹ if they are expressed in less than 10% or more than 90% of the cells. For larger datasets including 10X PBMC, Worm neuron, Human kidney and Mouse retina datasets, we filtered cells with fewer than one gene and retained genes expressed in at least one cell using Scanpy. For mouse brain, we excluded cells with fewer than 200 genes and mitochondrial genes with a UMI greater than 5%. Genes expressed in less than 3 cells were also removed. For TAM FACS, we retained genes expressed in at least 3 cells and cells with no less than 250 expressed genes and 5000 counts. For MCA, cells with fewer than 100 genes and genes with less than 3 cells were excluded. After filtering, raw count matrix was normalized and log-transformed to detect highly variable genes (HVG). Finally, Principal Component Analysis (PCA) was performed on the selected HVGs, and the top 50 PCs were retained for clustering. For COVID-19, we downloaded the processed data provided by the authors.

Note that two optional steps of data preprocessing, i.e., normalization and selection of HVGs, can potentially affect the clustering results^{32, 33}. Therefore, we compared the clustering accuracies of different methods both with and without these two steps (**Supplementary Fig. 6**).

Data simulation. Simulating ultra-large scRNA-seq data that mimics realistic data is challenging. We conducted our simulations using the PCA-transformed Mouse brain dataset as a reference, and jittering the transformed dataset by adding random noise following uniform distribution over $[-\mu, \mu]$ for some parameter $\mu > 0$ (for more information, see the *jitter* function in R). The parameter a is estimated from the data. Specifically, we eliminated duplicates, sorted in ascending order, and computed the first-order differences on 1D-reshaped data. Then we identified the least value (ϵ) among the differences, and used $1/\epsilon$ to calculate the distribution parameter μ . The parameter μ is estimated to be 0.00199986 in the transformed dataset. We repeated the jittering process multiple times, and merged all replicates as a reservoir of simulations with 40 million cells. Finally, we obtained simulation datasets with varying numbers of cells from 10,000 to 40 million, by randomly drawing from this reservoir.

Spectral clustering. Spectral clustering is a popular clustering algorithm originated in spectral graph theory³⁴. Given a graph $G = \{X, E, S\}$, where $X = \{x_1, \dots, x_N\}$ is a set of data points, E is a set of edges and $S = [S_{in}]_{i,n=1,2,\dots,N}$ is a weighted adjacency or similarity matrix, spectral clustering aims to divide the graph into disjoint subgraphs in which the within-group edge weights are maximized while the between-group edge weights are minimized. A typical spectral clustering algorithm constitutes the following main steps: 1) constructing an adjacency matrix S for data points based on certain distances (e.g., Euclidean, cosine); 2) computing the graph Laplacian matrix, i.e., $L = D - S$, where D is the degree matrix of the graph, a diagonal matrix with diagonal elements equal to the row sums of S ; 3) calculating the eigenvectors corresponding to the K smallest eigenvalues of the (normalized) Laplacian and arranging them in a matrix V by columns; 4) clustering the row-normalized V into K groups using conventional clustering algorithms, such as k-means or hierarchical clustering. Spectral clustering has several variants by using different forms of the Laplacian matrix¹⁰. Among them, Normalized cut (Ncut) is the most widely adopted method³⁵.

Secuer. Our method is comprised of four steps: 1) identifying anchors; 2) estimating the number of clusters; 3) applying the MAKNN algorithm to construct the bipartite graph between anchors and cells; 4) partitioning the bipartite graph partitioning. Among them, the step of identifying anchors to generate an adjacency matrix of cell-by-anchor to replace the original dense similarity matrix is key for drastically improving the clustering runtime and memory usage. The vanilla spectral clustering requires: (1) $O(N^2d)$ time to build the adjacency matrix and (2) $O(N^3)$ time to solve the eigenproblem (where N and d are sample sizes and the number of dimensions, respectively)³⁶. In contrast, Secuer reduces the time complexity to $O(Np^{\frac{1}{2}}d)$ in (1) by using the bipartite graph representation, and reduces the time complexity to $O(NK(K+k) + p^3)$ ^{37, 38} in (2) by using transfer-cuts (T-cut)³⁷ on the weighted bipartite graph to solve the eigenproblem, where k is the number of neighboring anchors and K is the estimated number of cell clusters.

Identifying anchors. Given a dataset $X = \{x_i\}_{i=1,\dots,N}$, where $x_i \in \mathbb{R}^d$ represents a cell with d features, we selected p (default by 1000) anchors to bypass computing the original large and dense similarity matrix. The idea behind this step is to use a small set of landmark points to approximately represent the underlying geometry of the data. In detail, we first randomly selected p' candidate cells from all N cells such that $p < p' \ll N$, and then group candidate cells into p clusters by k-means clustering. The final anchors are the centroids of the p clusters, denoted as $r = \{r_1, r_2, \dots, r_p\}$. Note that, for datasets with cells less than 10,000, we applied k-means on the dataset directly to identify anchors.

Estimating the number of clusters. The number of clusters is usually given *a priori* for vanilla spectral clustering algorithms. However, the true number of cell types is

seldomly available in practice. In the current version of Secuer, we implemented two approaches for estimating the number of clusters. Inspired by community-detection algorithms that infer the number of clusters using a resolution parameter, we constructed a graph with only anchors as nodes and estimate the number of clusters by the community-detection-based approach used in Louvain algorithm.

Another option is to use the bipartite graph between anchors and cells. It is proven that the number of near-zero eigenvalues of the graph Laplacian matrix equals the number of the connected components of the underlying graph¹⁰. Inspired by this fact, we designed an approach consisting of the following five steps: 1) sorting the eigenvalues of the bipartite graph Laplacian matrix in ascending order; 2) dividing all the eigenvalues into 100 equal-sized bins $\mathcal{H} = \{(L_u, R_u) | u = 1, 2, \dots, 100\}$ and count the number C_u of eigenvalues falling into each bin; 3) computing the gap values Δ between consecutive bin pairs with $C_u > 0$, denoted as $\Delta = \{L_{u'+1} - R_{u'} | u': C_{u'} > 0\}$, and identify the α -th greatest values Δ_α in Δ (with default value set as $\alpha = 4$ by empirical experience from simulations and data analysis); 4) determining the bins with gap values greater than Δ_α and obtain $u^* = \operatorname{argmax}_{u'} \{R_{u'} | L_{u'+1} - R_{u'} > \Delta_\alpha\}$; 5) estimating the number of clusters by the number of eigenvalues falling into all bins with $u \leq u^*$.

The MAKNN algorithm. Given p anchors, we aimed to construct an $N \times p$ similarity matrix S between all N cells and p anchors. However, this step can be computational expensive in terms of both runtime and memory usage for ultra-large datasets. To alleviate this problem, we used a modified approximate KNN algorithm to improve the computational efficiency. For large datasets, instead of building a large and dense adjacency matrix, the modified method aims to find k nearest anchors approximately for each cell to build a sparse adjacency matrix of cell-to-anchor. Taking a cell x_i as an example:

- i) All p anchors are grouped into o clusters using k-means, denoted as $\omega_1, \omega_2, \dots, \omega_o$.
- ii) Cell x_i is then assigned to the closest cluster $\omega_i^{(i)}$ based on the Euclidean distance between cell x_i and all cluster centers.
- iii) Find the nearest anchor of cell x_i in $\omega_i^{(i)}$ denoted as $p^{(i)}$.
- iv) Apply KNN to p anchors to obtain the k' (default as $10 \times k$) nearest neighbors of each anchor such that $k < k'$.
- v) Obtain the k nearest anchors of cell x_i based on the Euclidean distance between x_i and the k' nearest anchors of $p^{(i)}$.

In the above steps, we only need to calculate the k' nearest neighbors of p anchors. Then the neighbors of the anchor closest to the cell x_i are treated as neighbors of that cell. The time complexity of this procedure is $O(podt + ptd + N \frac{p}{o} d + pdk +$

$Nkd)$, with the least value when o is $p^{\frac{1}{2}}$, where t is the number of iterations of k-

means. Due to $k \ll p \ll N$, $O(Np^{\frac{1}{2}}d)$ term dominates the time.

We next used a locally-scaled Gaussian kernel to measure the distance between cells and anchors, and obtain an $N \times p$ adjacency matrix B with each row only keeping k nonzero elements as

$$B = [b_{ij}], i = 1, 2, \dots, N, j = 1, 2, \dots, p,$$

$$b_{ij} = \begin{cases} \exp\left(-\frac{\|x_i - r_j\|^2}{2\sigma_i^2}\right), & \text{if } r_j \in N_k(x_i), \\ 0, & \text{otherwise,} \end{cases}$$

where $N_k(x_i)$ represents the k nearest anchors of cell x_i , and σ_i is the average distance between cell x_i and its k nearest anchors.

Bipartite graph partitioning. Putting all cells and anchors together, we constructed a bipartite graph $G_b = \{X, r, W\}$, where W is a $(N + p) \times (N + p)$ weighted adjacency matrix, denoted as:

$$W = \begin{bmatrix} 0 & B \\ B' & 0 \end{bmatrix}.$$

Then spectral clustering is performed to partition the graph by solving the generalized eigen-problem:

$$Lv = \gamma Dv, \quad (1)$$

where $L = D - W$ is the Laplacian matrix, $D = \begin{bmatrix} D_X & 0 \\ 0 & D_p \end{bmatrix}$ is the degree matrix of the graph G_b .

For large datasets in which the number of cells is far greater than the number of anchors, G_b is an unbalanced bipartite graph. We thus employed an efficient eigen-decomposition method T-cut³⁷, which turns the problem (1) into a computational eigenproblem:

$$L_p z = \lambda D_p z, \quad (2)$$

where $L_p = D_p - W_p$, $W_p = B' D_N^{-1} B$. Note that $D_p = \text{diag}(B' \mathbf{1}_p) = \text{diag}(W_p \mathbf{1}_p)$.

Here L_p is the Laplacian matrix of the graph $G_p = \{r, W_p\}$, and $\mathbf{1}_p = [1, 1, \dots, 1]^T$.

Li et al proved that the solution of the eigen-problem (1) on graph G_p and the solution of the eigen-problem (2) on bipartite graph G_b are equivalent³⁷. Let $\{(\lambda_e, z_e)\}_{e=1}^K$ be the first K eigenpairs of (2), where $0 = \lambda_1 < \lambda_2 < \dots < \lambda_K < 1$, and $\{(\gamma_e, f_e)\}_{e=1}^K$ be the first K eigenpairs of (1), where $0 \leq \gamma_e < 1$. According to Li et al.³⁷, we have the following

$$\gamma_e(2 - \gamma_e) = \lambda_e,$$

$$v_e = \begin{bmatrix} \xi_e \\ z_e \end{bmatrix},$$

where $\xi_e = \frac{1}{1 - \gamma_e} P z_e$, and $P = D_N^{-1} B$ is the associated transition probability matrix

from cells to anchors.

After normalizing the matrix $T = [\xi_1, \dots, \xi_K]_{N \times K}$ to unit length, k-means is applied to the rows of normalized matrix to obtain the final clustering result. Note that k-means can be replaced by other clustering algorithms such as DBSCAN or hierarchical clustering. However, these methods are generally less efficient than k-means.

Secuer-consensus. Taking advantage of the computational efficiency of Secuer, we proposed a consensus clustering method Secuer-consensus, which aggregates multiple clustering outputs from Secuer to boost the clustering stability and accuracy. The implementation is as follows. First, M different base clustering results are obtained from Secuer, by varying the selection of anchors, the number of clusters, and the distance metrics between anchors and cells (Euclidean or cosine). Denote all the clusters in M base clustering results as $C = \{c_1^1, \dots, c_1^{K_1}, c_2^1, \dots, c_2^{K_2}, \dots, c_M^1, \dots, c_M^{K_M}\}$, where K_m is the number of clusters in the m -th clustering result and $c_m^{e_m}$ is the e_m -th cluster of the base clustering result c_m . Then, a bipartite graph $G_{xc} = \{X, C, \tilde{W}\}$ is constructed, in which the nodes are the cells and clusters and \tilde{W} is an $(N + M_c) \times (N + M_c)$ adjacency matrix indicating whether a cell belongs to a cluster, where $M_c = \sum_{m=1}^M K_m$. An edge only appears between a cell and the clusters to which the cell belongs and no edges between different cells or between different clusters are allowed. \tilde{W} can be written as:

$$\tilde{W} = \begin{bmatrix} 0 & \tilde{E} \\ \tilde{E}' & 0 \end{bmatrix},$$

$$\tilde{E}_{iK_{m-1}+e_m} = \begin{cases} 1, & x_i \in c_m^{e_m} \\ 0, & \text{otherwise} \end{cases},$$

$$1 \leq e_m \leq K_m, K_0 = 0,$$

where \tilde{E} is an $N \times M_c$ matrix.

Similar to the Bipartite graph partitioning section, we next solved the eigenvalue of graph Laplacian of G_{xc} by T-cut. That means solving the following eigenproblem:

$$\tilde{L}\tilde{v} = \tilde{\gamma}\tilde{D}\tilde{v}, \quad (3)$$

where $\tilde{L} = \tilde{D} - \tilde{E}$, and \tilde{D} is the degree matrix.

The eigen-problem in (3) is equivalent to solving the following problem,

$$L_c\tilde{z} = \tilde{\lambda}D_c\tilde{z}, \quad (4)$$

where $E_c = \tilde{E}'\tilde{D}\tilde{E}$ is the adjacency matrix, $D_c = \text{diag}(E_c\mathbf{1}_N)$ and $L_c = D_c - E_c$ are the degree matrix and Laplacian matrix of G_c , respectively

Let $\{(\tilde{\lambda}_e, \tilde{z}_e)\}_{e=1}^K$ be the first K eigenvalues and eigenvectors of (4), where

$0 = \tilde{\lambda}_1 < \tilde{\lambda}_2 < \dots < \tilde{\lambda}_K < 1$. Further let $\{(\tilde{\gamma}_e, \tilde{f}_e)\}_{e=1}^K$ be the first K eigenpairs of (3), where $0 \leq \tilde{\gamma}_e < 1$. Then we have:

$$\tilde{\gamma}_e(2 - \tilde{\gamma}_e) = \tilde{\lambda}_e,$$

$$\tilde{v}_e = \begin{bmatrix} \tilde{\xi}_e \\ \tilde{z}_e \end{bmatrix},$$

where $\tilde{\xi}_e = \frac{1}{1-\tilde{\gamma}_e} \tilde{P} \tilde{Z}_e$, and $\tilde{P} = D_c^{-1} \tilde{E}$.

Then k-means is applied to the rows of normalized matrix $\tilde{T} = [\tilde{\xi}_1, \dots, \tilde{\xi}_K]_{N \times K}$ to obtain the final clustering result.

Distance metrics: Denote $x_{ig}, i = 1, \dots, N, g = 1, \dots, d$ as the gene expression level of the cell i in gene j . We used the following Euclidean and cosine distances as candidate distance metrics to build the bipartite graph between cells and anchors:

$$D_{Euclidean}(x_i, x_n) = \sqrt{\sum_{g=1}^d (x_{ig} - x_{ng})^2},$$

$$D_{cosine}(x_i, x_n) = 1 - \frac{\sum_{g=1}^d x_{ig} x_{ng}}{\sqrt{\sum_{g=1}^d x_{ig}^2} \sqrt{\sum_{g=1}^d x_{ng}^2}}.$$

Clustering metrics. We compared the clustering accuracy of different methods using the adjusted rand index (ARI)¹¹ and normalized mutual information (NMI)¹², which are widely used indices for evaluating the clustering performance when the reference or the true cluster labels are known. ARI is defined as

$$ARI = \frac{\sum_{\zeta, \tau} \binom{N_{\zeta\tau}}{2} - [\sum_{\zeta} \binom{N_{\zeta}}{2} \sum_{\tau} \binom{N_{\tau}}{2}] / \binom{N}{2}}{\frac{1}{2} [\sum_{\zeta} \binom{N_{\zeta}}{2} + \sum_{\tau} \binom{N_{\tau}}{2}] - [\sum_{\zeta} \binom{N_{\zeta}}{2} \sum_{\tau} \binom{N_{\tau}}{2}] / \binom{N}{2}},$$

where N is the total number of cells, and $N_{\zeta\tau}$ represents the number of cells that are shared by the predicted cluster ζ and true label τ , N_{ζ} and N_{τ} are the number of cells in the predicted cluster ζ and true label τ , respectively. NMI is defined as

$$NMI = \frac{\sum_{\zeta, \tau} P_{\zeta\tau} \log \frac{P_{\zeta\tau}}{P_{\zeta} P_{\tau}}}{(-\sum_{\zeta} P_{\zeta} \log P_{\zeta} - \sum_{\tau} P_{\tau} \log P_{\tau}) / 2},$$

where $P_{\zeta\tau} = \frac{N_{\zeta\tau}}{N}$, $p_{\zeta} = \frac{N_{\zeta}}{N}$ and $P_{\tau} = \frac{N_{\tau}}{N}$. Higher ARI or NMI indicates better clustering result.

Data availability

The datasets in this study are all publicly available: Biase, Yan, Goolam, Deng, Pollen and kolodziejczyk (<https://hemberg-lab.github.io/scRNA.seq.datasets/>), Worm neuron, 10X PBMC, CITE PBMC, and Mouse retain and Human kidney (<https://github.com/ttgump/scDCC/tree/master/data>), TAM FACS (https://figshare.com/projects/Tabula_Muris_Senis/64982), MCA (https://figshare.com/articles/dataset/MCA_DGE_Data/5435866), and COVID19 (<https://drive.google.com/file/d/1IwWcn4WYKgNbz4DpNweM2cKx1x1hbM0/view>).

Code availability

Python implementation of Secuer is available on GitHub

(<https://github.com/nanawei11/Secuer>).

References

1. Kolodziejczyk, A.A., Kim, J.K., Svensson, V., Marioni, J.C. & Teichmann, S.A. The technology and biology of single-cell RNA sequencing. *Mol. Cell* **58**, 610-620 (2015).
2. Ziegenhain, C. et al. Comparative analysis of single-cell RNA sequencing methods. *Mol. cell* **65**, 631-643. e634 (2017).
3. Wang, D. & Bodovitz, S. Single cell analysis: the new frontier in 'omics'. *Trends Biotechnol.* **28**, 281-290 (2010).
4. Brbić, M. et al. MARS: discovering novel cell types across heterogeneous single-cell experiments. *Nat. Methods* **17**, 1200-1206 (2020).
5. Ren, X. et al. COVID-19 immune features revealed by a large-scale single-cell transcriptome atlas. *Cell* **184**, 1895-1913. e1819 (2021).
6. Duò, A., Robinson, M.D. & Sonesson, C. A systematic performance evaluation of clustering methods for single-cell RNA-seq data. *F1000Res.* **7** (2018).
7. Kiselev, V.Y. et al. SC3: consensus clustering of single-cell RNA-seq data. *Nat. methods* **14**, 483-486 (2017).
8. Blondel, V.D., Guillaume, J.-L., Lambiotte, R. & Lefebvre, E. Fast unfolding of communities in large networks. *J Stat Mech.* **2008**, P10008 (2008).
9. Traag, V.A., Waltman, L. & van Eck, N.J. From Louvain to Leiden: guaranteeing well-connected communities. *Sci. Rep.* **9**, 1-12 (2019).
10. Von Luxburg, U. A tutorial on spectral clustering. *Statistics and computing* **17**, 395-416 (2007).
11. Hubert, L. & Arabie, P. Comparing partitions. *J Journal of classification* **2**, 193-218 (1985).
12. Strehl, A. & Ghosh, J. Cluster ensembles --- a knowledge reuse framework for combining multiple partitions. *J. Mach. Learn. Res.* **3**, 583-617 (2003).
13. McInnes, L., Healy, J. & Melville, J. Umap: Uniform manifold approximation and projection for dimension reduction. *J arXiv preprint arXiv:03426* (2018).
14. Xie, K., Huang, Y., Zeng, F., Liu, Z. & Chen, T. scALDE: clustering of large-scale single-cell RNA-seq data reveals putative and rare cell types. *NAR genomics bioinformatics* **2**, lqaa082 (2020).
15. Tian, T., Wan, J., Song, Q. & Wei, Z. Clustering single-cell RNA-seq data with a model-based deep learning approach. *Nat. Mach. Intell.* **1**, 191-198 (2019).
16. Biase, F.H., Cao, X. & Zhong, S. Cell fate inclination within 2-cell and 4-cell mouse embryos revealed by single-cell RNA sequencing. *Genome Res.* **24**, 1787-1796 (2014).
17. Deng, Q., Ramsköld, D., Reinius, B. & Sandberg, R. Single-cell RNA-seq reveals dynamic, random monoallelic gene expression in mammalian cells. *Science* **343**, 193-196 (2014).
18. Patel, A.P. et al. Single-cell RNA-seq highlights intratumoral heterogeneity in primary glioblastoma. *Science* **344**, 1396-1401 (2014).
19. Pollen, A.A. et al. Low-coverage single-cell mRNA sequencing reveals cellular heterogeneity and activated signaling pathways in developing cerebral cortex. *Nat. Biotechnol.* **32**, 1053-1058 (2014).
20. Goolam, M. et al. Heterogeneity in Oct4 and Sox2 targets biases cell fate in 4-cell mouse

- embryos. *Cell* **165**, 61-74 (2016).
21. Innes, B.T. & Bader, G.D. scClustViz—Single-cell RNAseq cluster assessment and visualization. *F1000Res.* **7** (2018).
 22. Zheng, G.X.Y. et al. Massively parallel digital transcriptional profiling of single cells. *Nat. Commun.* **8**, 14049 (2017).
 23. Young, M.D. et al. Single-cell transcriptomes from human kidneys reveal the cellular identity of renal tumors. *Science* **361**, 594-599 (2018).
 24. Shekhar, K. et al. Comprehensive Classification of Retinal Bipolar Neurons by Single-Cell Transcriptomics. *Cell* **166**, 1308-1323.e1330 (2016).
 25. Mimitou, E.P. et al. Multiplexed detection of proteins, transcriptomes, clonotypes and CRISPR perturbations in single cells. *Nat. methods* **16**, 409-412 (2019).
 26. Cao, J. et al. Comprehensive single-cell transcriptional profiling of a multicellular organism. *Science* **357**, 661-667 (2017).
 27. Han, X. et al. Mapping the Mouse Cell Atlas by Microwell-Seq. *Cell* **172**, 1091-1107.e1017 (2018).
 28. Zhang, M.J., Pisco, A.O., Darmanis, S. & Zou, J. Mouse aging cell atlas analysis reveals global and cell type-specific aging signatures. *eLife* **10**, e62293 (2021).
 29. Tian, T., Zhang, J., Lin, X., Wei, Z. & Hakonarson, H. Model-based deep embedding for constrained clustering analysis of single cell RNA-seq data. *Nat. Commun.* **12**, 1873 (2021).
 30. Consortium, T.M. A single cell transcriptomic atlas characterizes aging tissues in the mouse. *Nature* **583**, 590 (2020).
 31. Wolf, F.A., Angerer, P. & Theis, F.J. SCANPY: large-scale single-cell gene expression data analysis. *Genome Biol.* **19**, 1-5 (2018).
 32. Tian, L. et al. Benchmarking single cell RNA-sequencing analysis pipelines using mixture control experiments. *Nat. methods* **16**, 479-487 (2019).
 33. Germain, P.-L., Sonrel, A. & Robinson, M.D. pipeComp, a general framework for the evaluation of computational pipelines, reveals performant single cell RNA-seq preprocessing tools. *Genome Biol.* **21**, 1-28 (2020).
 34. Chung, F.R. & Graham, F.C. Spectral graph theory, Vol. 92. (American Mathematical Soc., 1997).
 35. Shi, J. & Malik, J. Normalized cuts and image segmentation. *IEEE Trans. Pattern Anal. Mach. Intell.* **22**, 888-905 (2000).
 36. Chen, X. & Cai, D. in Large scale spectral clustering with landmark-based representation (Twenty-fifth AAAI conference on artificial intelligence, 2011).
 37. Li, Z., Wu, X.-M. & Chang, S.-F. in Segmentation using superpixels: A bipartite graph partitioning approach 789-796 (2012 IEEE conference on computer vision and pattern recognition, 2012).
 38. Huang, D. et al. Ultra-scalable spectral clustering and ensemble clustering. *IEEE Trans. Comput.* **32**, 1212-1226 (2019).

Supplementary Files

Supplementary table 1 scRNA-seq Datasets used in this study.

Dataset	Protocols	#Cells	#Genes	K			Source
				Refere nce	Louvain	Secuer	
Biase	SMART- seq	49	3922	3	3	3	Biase, et al. GSE57249
Yan	TruSeq DNA	90	2903	7	3	3	Yan, et al., 2013 GSE36552
Goolam	Smart- Seq2	124	3212	5	3	5	Goolam, et al. E-MTAB- 3321
Deng	SMART- seq	268	3028	10	6	9	Deng, et al. GSE46719 Pollen, et al.
Pollen	SMART- seq	301	3942	11	8	9	https://scrnaseq-public- datasets.s3.amazonaws.co m/scater-objects/pollen.rds KolodziejczykESData
kolodziejc zyk	SMART- seq	704	3212	3	6	7	function of the R package scRNAseq.
Worm neuron	sci-RNA- seq	4186	1525	10	34	28	https://atlas.gs.washington. edu/worm-rna/docs/
CITE PBMC	CITE-seq	3,762	255	15	14	15	https://github.com/ttgump/ scDCC/tree/master/data
10X PBMC	10X Genomics	4,217	1,285	8	13	12	Zheng, et al. https://github.com/ttgump/ scDCC/tree/master/data
Human kidney	10X Genomics	5685	5707	11	26	17	Young, et al. https://github.com/xuebalia ng/scziDesk/tree/master/da taset/Young
Mouse retina	Drop-seq	27499	1639	19	20	16	Shekhar, et, al. GSE81905
TAM FACS	Smart- seq2	110823	2846	23	49	25	https://figshare.com/article s/dataset/tms_gene_data_rv 1/12827615
MCA	Microwell -seq	325486	2940	47	52	32	Han, et al. https://figshare.com/article s/dataset/MCA_DGE_Data /5435866

Mouse brain	10X Genomics	1011462	1376	19	28	16	https://support.10xgenomics.com/single-cell-gene-expression/datasets/1.3.0/1M_neurons Ren, et al.
COVID-19	10x Genomics	1462702	27943	12/64	45	14	https://drive.google.com/file/d/1IwWcn4WYKgNbz4DpNweM2cKxlx1hbM0/view

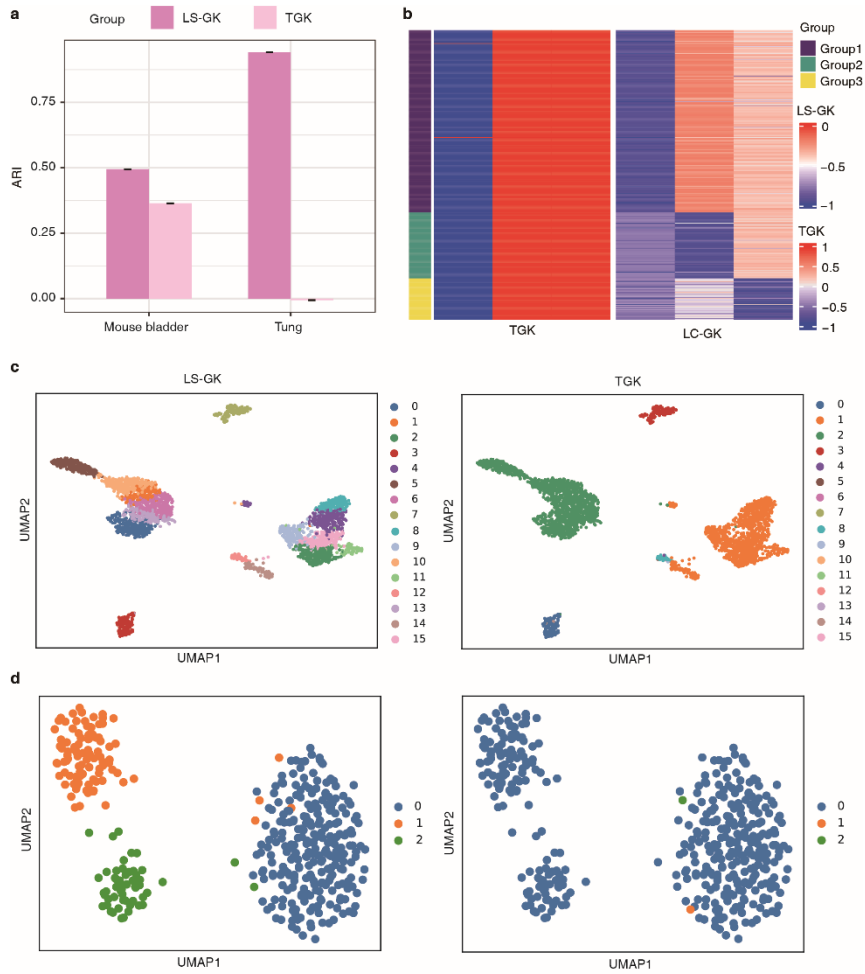


Fig. S1 Evaluation of locally-scaled Gaussian kernel function. a, Comparison of the ARI scores in two datasets (Mouse bladder and Tung) when using a traditional Gaussian kernel (TGK) and a locally-scaled Gaussian kernel (LS-GK). Mouse bladder dataset with 2746 cells and 2264 genes is the bladder tissue from MCA datasets, Tung dataset is obtained from the *Splatter* R package. **b**, Heatmap showing the eigenvectors of the bipartite graph Laplacian on the Tung dataset using the two different kernel functions, where rows represent cells and columns represent the M first eigenvectors. The ground-truth labels are plotted as groups. **c, d**, The UMAP of clustering results on the two datasets.

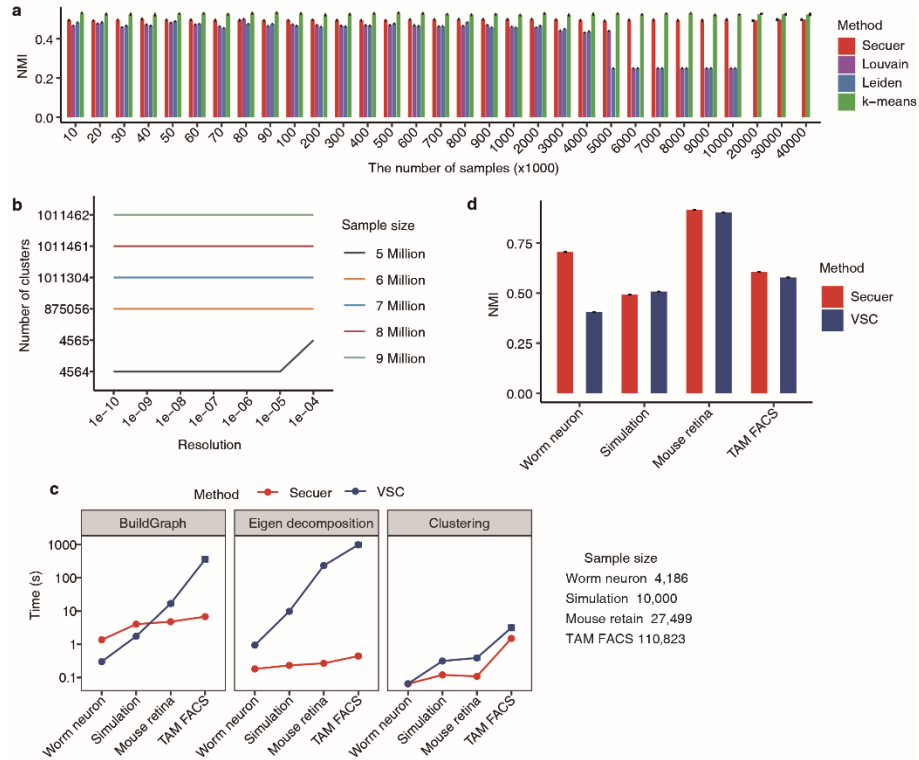


Fig. S2 Performance of Secuer and the other methods on simulated datasets and Comparison of consuming time with vanilla spectral clustering. **a**, The NMI of different methods on simulated datasets with different sample sizes. **b**, The number of clusters estimated by Louvain in five simulated datasets with sample sizes ranging from 5 million to 9 million under different resolutions (x-axis). **c**, We divided the entire clustering procedure into three steps and showed the runtime of each step taken by Secuer and vanilla spectral clustering (VSC) on four datasets, including Worm neuron, Simulation data (10,000 samples), Mouse retina and TAM FACS with the number of cells ranging from 4,217 to 110,823. **d**, The NMI of two methods on the four datasets.

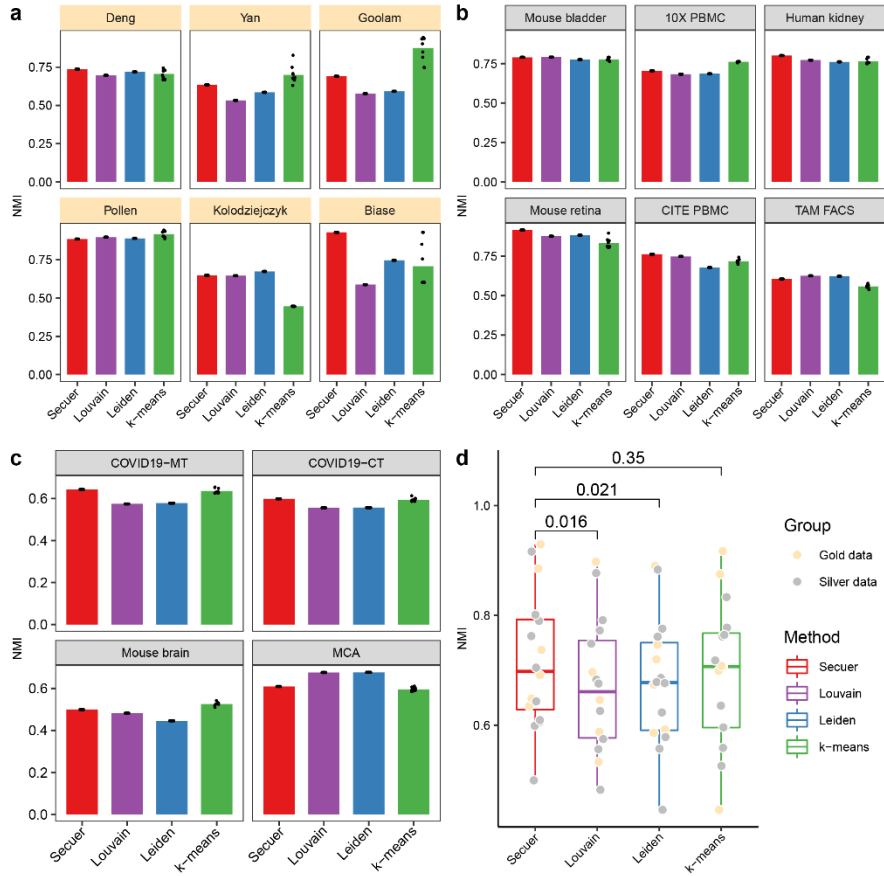


Fig. S3 The performance of the different methods by NMI metrics on all 15 datasets. **a-c**, The NMI of the different methods on six gold standard datasets (**a**), six silver standard datasets (**b**), and the three large datasets (**c**). **d**, The summary of NMI of the different methods on 15 datasets.

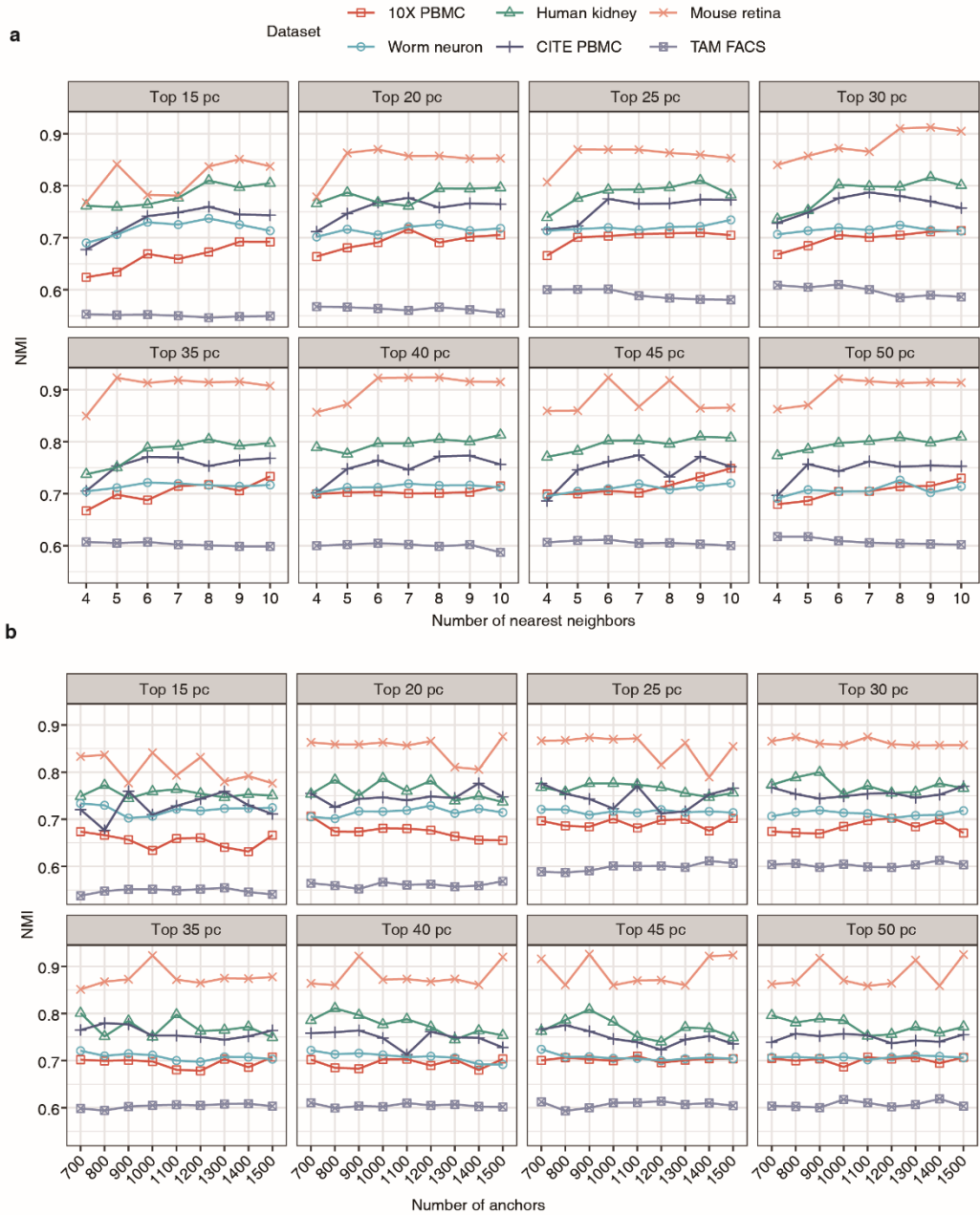


Fig. S4 The Secuer parameters benchmarked in six datasets. a, The NMIs for six datasets are computed, over different top numbers of principal components (pc), different number of nearest neighbors in MAKNN, and different number of anchors. **b,** The NMIs for six datasets are computed over different numbers of principal components and different numbers of anchors. Different panels represent different number of principal components.

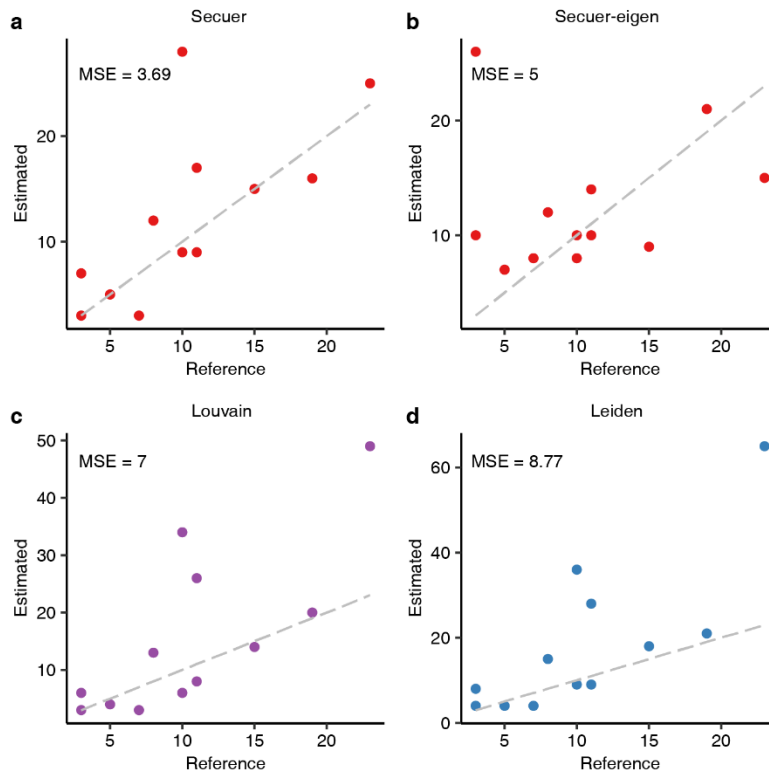
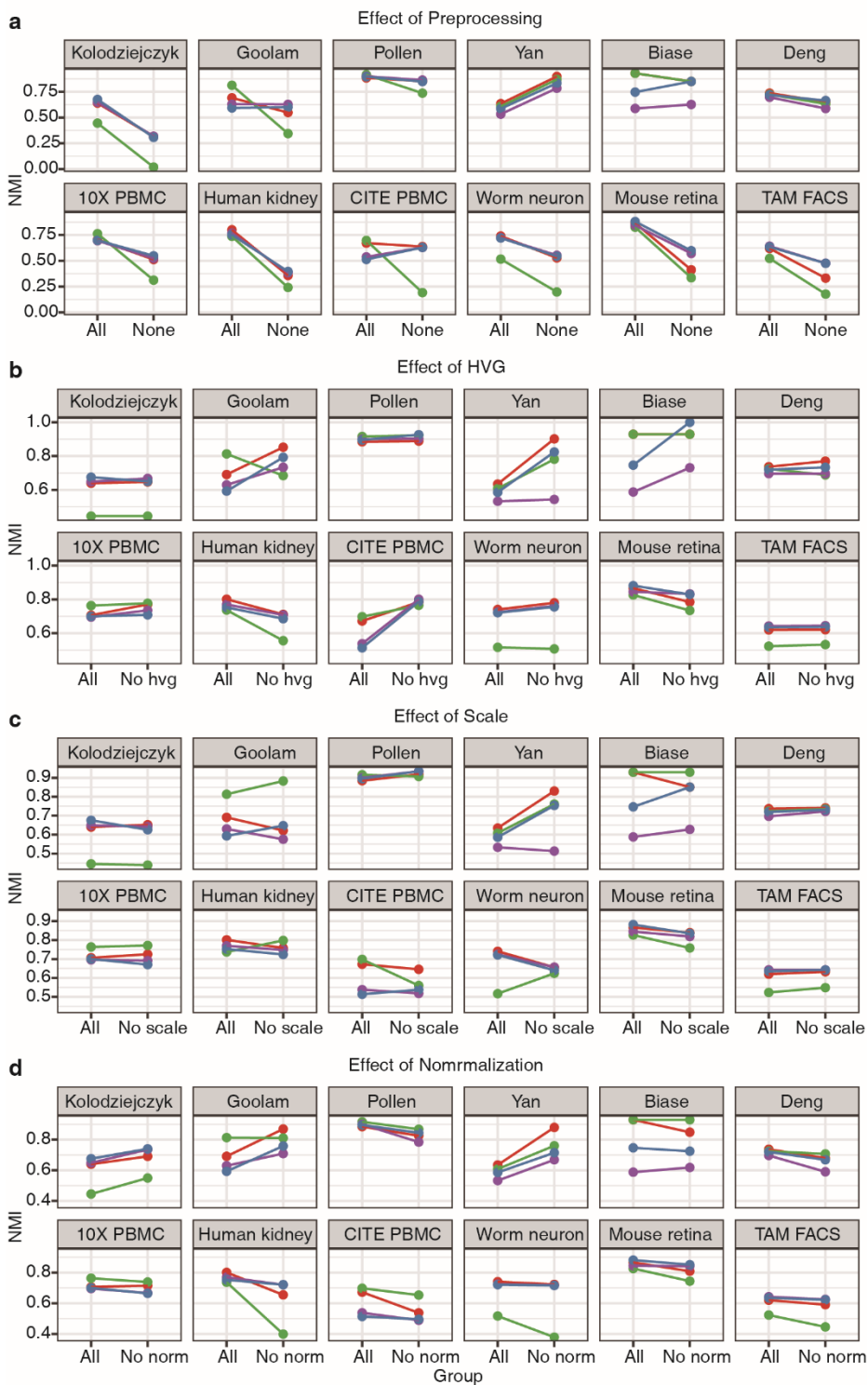


Fig. S5 The accuracy of the number of clusters estimated by different methods on the twelve gold/silver standard datasets. a-c. The Pearson correlation between the estimated number of clusters and the ground-truth (reference) across different methods: Secuer: based on the community detection on graph of anchors. **(a)**, Secuer-eigen: based on the eigenvalues of bipartite graph between cells and anchors **(b)** (see Methods), Louvain **(c)**, and Leiden **(d)**. The mean absolute error (MSE) for each method is shown in the top left corner of the plot.

Method — Secuer — k-means — Louvain — Leiden



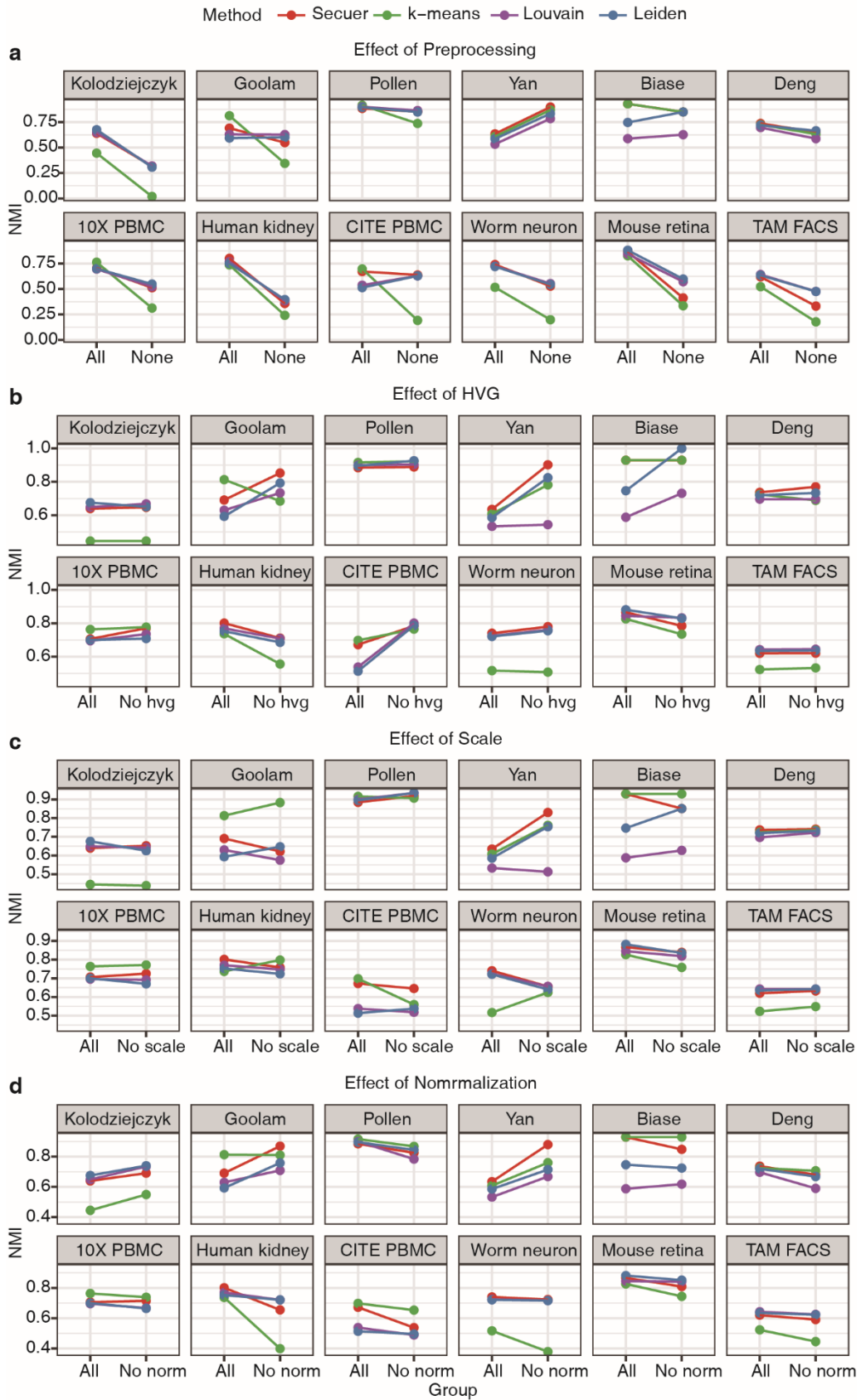


Fig. S6 The influence of the data preprocessing steps on clustering accuracy. a, Clustering performance with and without preprocessing, in which "ALL" refers to using all four preprocessing steps including normalization, logarithmic transformation, selection of high variable genes (HVG)

and scaling (zero mean and equal variance), and 'None' refers to omitting all four steps. Comparison of clustering accuracy between removing one of the steps and 'ALL', including removing normalization (**b**), logarithmic transformation (**c**), selection of high variable genes (**d**) and scaling (**e**).

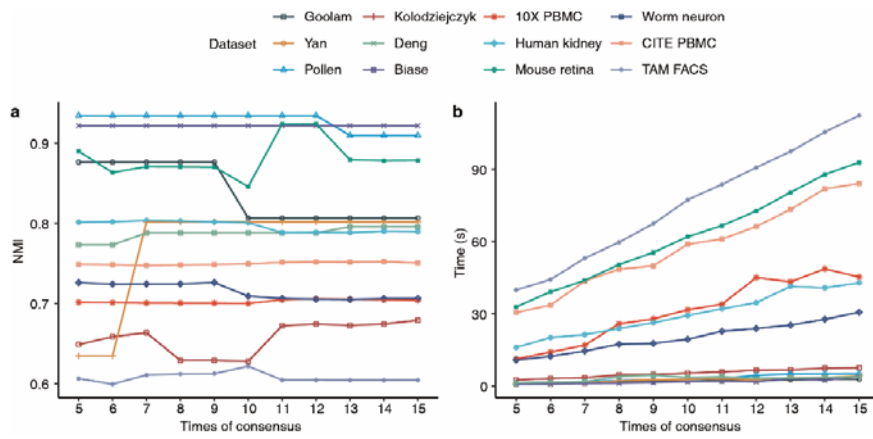


Fig. S7 The Secuer-consensus parameters benchmarked on twelve datasets. a, Clustering accuracy quantified by NMI vs. the number of cluster (M) outputs of Secuer fed into Secuer-consensus over different datasets. **b,** Runtime vs. M over different datasets.